

Highly correlated electronic bounding and spin effect: confirmation of an autodetaching state of O^- .

M. M. Sant'Anna,¹ Martínez-Calderón A. A.,^{2,*} Ginette Jalbert,¹ A. B. Rocha,^{3,†} and G. Hinojosa^{2,‡}

¹*Instituto de Física, Universidade Federal do Rio de Janeiro,
Caixa Postal 68528, Rio de Janeiro, - RJ 21941-972, Brazil.*

²*Instituto de Ciencias Físicas, Universidad Nacional Autónoma de México,
Avenida Universidad s/n, Col. Chamilpa, Cuernavaca, Morelos, 62210 Mexico.[§]*

³*Instituto de Química, Universidade Federal do Rio de Janeiro,
Caixa Postal 68528, Rio de Janeiro, - RJ 21941-972, Brazil.*

(Dated: February 18, 2026)

Reproduced from: Phys. Rev. A, Vol. 112, 052823, Published Nov., 20th 2025, with the permission of AIP Publishing. This article may be downloaded for personal use only. Any other use requires prior permission AIP Publishing. The article may be found at: DOI: <https://doi.org/10.1103/2st9-v5h1>.

The existence of an auto-detaching state of O^- with a lifetime on the scale of a hundred nanoseconds is demonstrated both experimentally and theoretically. The O^- lifetime values are determined using two recently developed methods. The experimental approach is based on a derivation from measured electron-loss cross sections combined with time-of-flight spectrometry. For the theoretical approach, the continued Green's function within the formalism of Fano-Feshbach is applied. We present the measured lifetime value of 100 ± 10 ns. The calculated lifetime value is 75 ns, and is associated with the $(2p^33s^2)^4S$ state of O^- . We discuss how the existence of a 100-ns-lifetime oxygen metastable anion can impact the modeling of oxygen-containing systems.

The electronic structure of negative ions is dominated by electronic correlation effects [1–3]. Unlike atoms and positive ions, anions present bound-state spectra with a finite number of energy levels. In this respect, they are more alike to nuclei than to atoms or positive ions. The search and detection of anions in space and in Earth's atmosphere, especially H^- and O^- , triggered the early development of theoretical methods for studying their electronic structure, in configurations ranging from the ground state and possible singly-excited states [4–7] to doubly-excited self-detaching states [8, 9]. While for H^- some attempts to measure the lifetimes of auto-detaching states have been made [10–12], for O^- , there are no reports of similar efforts.

The interaction between slow anions and atomic or molecular partners, either neutral or charged, gives rise to the so-called chemistry of negative ions [13]. The creation and destruction of O^- in a chemical environment are related to several processes, including atomic collisions, dissociative electron attachment (DEA) to molecules [14–16], and photodetachment [17]. These interaction processes occur within different time scales. The analysis of the role played by excited states in these systems depends on the knowledge of the particular intrinsic time scale of the state decay. Therefore, incomplete knowledge of the auto-detaching states of O^- precludes a careful evaluation of their role in time-dependent

physical systems for which electronic excitation is possible.

On Earth, O^- is present in several physical systems, such as in earth's troposphere [18], in flames [19–21], and in sputtering plasmas [22]. Extraterrestrial planetary environments may involve O^- , like in the lower ionosphere of Mars [23] and in the ionosphere of Titan [24, 25]. In the latter case, O^- is described by Mukundan and Bhardwaj as a transient formed from photofragmentation of H_2O , reacting immediately with CH_4 or HCN to produce molecular anions, although they do not quantitatively discuss this immediacy [24]. Ayasli *et al.* [19] have recently observed long-lived transition states in low-energy $O^- + CH_4$ collisions. The presence of O^- long-lived excited states can influence reaction rates, affecting the genesis of molecular anions formed as byproducts of such transition states.

The K-shell photoexcitation of small molecules also produces O^- fragments. The photon-energy dependences of the produced O^- through photofragmentation of CO and H_2O show signatures of post-collision interaction [26, 27]. Linewidth measurements with CO target provide both, core-hole and vibrational of the order of 10 fs [26]. The post-collision interaction characteristic time, however, is not measured or calculated. The electron recapture process is inherent to PCI. If auto-ionizing excited states of O^- live long enough, they may influence the recapture dynamics. This example shows that measurements of lifetimes for O^- excited states are important not only for providing time scales but also for helping to choose which excited states should be considered in the theoretical modeling of physical systems producing O^- ions.

* amartinez@icf.unam.mx

† rocha@iq.ufrj.br

‡ hinojosa@icf.unam.mx

§ mms@if.ufrj.br

Lifetimes for anionic excited states are essential for testing time-dependent quantum calculation methods and for estimating the impact of excited states in relevant physical systems.

To our knowledge, there exists a lifetime measurement for the O⁻ K-shell excited 1s¹2s²2p⁶ state [28]. There are also lifetime calculations for the (1s²2s²2p⁵)²P_{1/2} state, which is different from the ground state (1s²2s²2p⁵)²P_{3/2} only in the fine structure (with $\Delta E = 0.022$ eV [1]), estimating a lifetime of the order of hours for that metastable state [29]. For valence shell states, we could not find in the literature any lifetime measurement values for the excited states of O⁻.

The existence of doubly excited autodetaching states of O⁻ has been known for decades [30]. The spectroscopy of these states is known from the detection of emitted photons or electrons in collisions involving the O⁻ projectile and several targets [31]. However, those measurements do not provide lifetime values, since linewidth-based measurements in general are limited by the instrumental resolution (e.g. [32]). In this letter we present a lifetime measurement for an O⁻ doubly excited state, obtained using a novel technique based on the O⁻ projectile time of flight. We also present an independent Fano-Feshbach formalism calculation that includes an analytic continuation.

The present experimental method has been described previously in some detail [33] in a derivation for the lifetime of a possible auto-detaching state of H⁻ [12]. When the present Eq. (6) for ${}^m\sigma$ is applied to the previous analysis for H⁻, a new value for the auto-detaching state of 25 ns \pm 3 ns is derived, which we compare with the only available value for τ of 17 ns by Drake [34] for the 2p²(³P) of H⁻. This particular state of H⁻ has been investigated before by Bunge and collaborators [35] and by Bylicki and Bednarz [36]. Single excited states of H⁻ are short-lived (of the order of 10⁻¹⁴ s [37]), and are unresolved in the present experiment.

I. THEORY

In a previous paper [38], two of us have developed a method to calculate the autoionization width from a discretized pseudospectrum. The method is based on the analytic continuation of the Green's function within the Fano-Feshbach formalism. This approach is commonly used in quantum mechanics and many-body theory to study complex systems and their behavior. The Green's function provides valuable insights into the density of states and other physical quantities. By analytically continuing the Green's function, we explore its behavior in different regions of the complex plane, revealing important features of the system. In brief, a pseudo spectrum is constructed from methods relying on a L^2 square-integrable basis set. The energy is extended to the complex plane and the analytical continuation is performed through Padé approximants or, equivalently, via contin-

ued fractions. The ionization width is obtained from the imaginary part of the complex energy.

In the present case, the same method is used to obtain the autodetachment lifetime. For O⁻, the pseudospectrum is calculated as follows. Initially, a full valence CASSCF method was used to obtain the lowest-lying doublet and quartet states. Then, these states are used as basis to diagonalize the full Breit-Pauli Hamiltonian in order to obtain the spin-orbit manifold, which is finally used as pseudo-spectrum. The corresponding energies are extended to the complex plane where the analytical continuation is performed. The basis set used in all calculations is aug-cc-pVTZ complemented by Kaufmann's continuum-like basis set. These continuum-like functions are essential to properly describe the pseudo-continuum part of the spectrum and is explicitly presented in ref [39].

II. EXPERIMENT

Here, we offer the advancement of the new method to derive lifetimes (τ) based on collision-induced total electron loss cross-sections (CS) measurement of the anionic projectile O⁻ on O₂ and on N₂ as a function of the projectile kinetic energy. To our knowledge, there exists only one previous experimental approach to derive lifetimes from cross-sections, in that case, from dissociative electron detachment cross-sections for diatomic-like molecules [40].

The present method consists of the application of two different well-established techniques for the measurement of electron loss cross sections, namely, the beam attenuation (BAT) and the signal growth rate (SGR). BAT is based on measuring the remaining negative ions from an O⁻ ion beam after interacting with a target gas. SGR consists of measuring the resulting neutral atoms of oxygen produced from the electron loss after the interaction.

In the following, a brief description of the experimental method is given. Negative ions were extracted from a quartz-made chamber [41], containing a mixture of high-purity O₂ and Ar gases, where a plasma was induced by an incandescent filament. The ion source chamber was operated at a maximum pressure of 20 Pa and, had an exit orifice of 1.0 mm diameter on a 100 V biased metallic cap. The negative ions were expelled toward a set of electrostatic lenses that focused them in a magnetic field region where the O⁻ ions were separated according to their mass-to-charge ratio.

Before and after the magnetic field's region, two sets of parallel plates installed perpendicularly to the ion-beam direction, were used to apply small electric fields to fine-tune the ion beam trajectory.

A well-collimated, single-species, monoenergetic, and, focused ion beam, with a width of ≈ 0.5 mm, enters a gas cell where the interaction of O⁻ and O₂ occurs in a time frame of a fraction of 10⁻¹⁵ s,

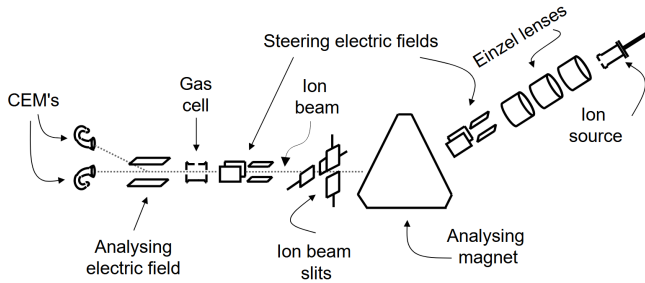
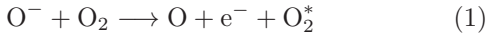


FIG. 1. Schematic diagram of the apparatus. Not to scale.



where the star is to indicate an unknown final internal state. High-purity O_2 gas was used. The resulting neutral oxygen atoms continued in their original trajectory towards a channel electron multiplier (CEM) located in the symmetry axis of the apparatus. The remaining O^- ions from the parent ion beam were diverted by a perpendicular electric field set (see Fig. 1) to steer the ions toward a second CEM installed off-axis of the accelerator symmetry axis. This Analyzing Electric Field will be referred to as AEF.

The transit time of a 1.0 keV O^- ion from the output of the ion source to the entrance of the gas cell was approximately 7 μs . The experiment was performed under high vacuum conditions so that the mean free path of the ion beam was larger than its total trajectory, except inside the gas cell.

To verify the full collection of the charged particles, the ion-beam intensity was measured as a function of the AEF intensity. The resulting profiles showed a plateau, indicating that their spatial spread was smaller than the width of the CEMs aperture after dispersion in the gas cell, therefore showing complete collection.

To check for the full collection of neutral atoms, we implemented a test with the lighter ion beam of H^- in the same apparatus [12]. The distance between the gas cell and the central CEM was modified between two experimental campaigns with a difference in aspect ratios of 18%, resulting in no measurable difference between the two sets of CS.

To verify similar detection efficiencies of both CEMs, the counting rate in the central CEM was measured with the AEF set to zero, corresponding to a total count rate of residual neutral atoms plus the O^- parent ion-beam counts. This counting rate was compared with the counting rates of the lateral CEM added to the central CEM's with the AEF on, confirming the total central CEM's count rate. This test was performed at each energy, under empty gas cell conditions. It is pointed out that this test also helps to reject any measurable electric field-induced electron detachment by the AEF since the total amount of particles remains unchanged with AEF on. The sys-

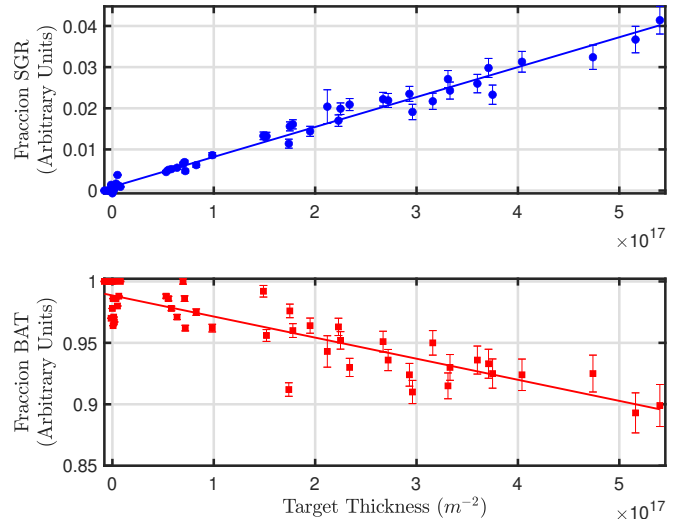


FIG. 2. Examples of the measured data at 2.5 keV. Relevant reduced signals of the SGR and BAT methods as a function of the target thickness. The top panel corresponds to SGR method and the lower panel corresponds to the BAT method. The electron detachment cross-section is given, at first order, by the slope for each curve.

tematic error of the cross-sections has been estimated to be 11% [42].

The measurement methods for the collision-induced total electron-loss cross section (CS) are based on the solutions to the fraction F equations for the three possible final projectile's charge states [43]. For instance, for the neutral atoms F is derived as, $F_0 = (I_0 - I_b)/I_i$ where I_0 is the signal count rate of oxygen atoms that resulted from the interaction with the gas, I_b is the ion-beam background count rate and I_i is the count rate of the initial parent ion beam with an empty gas cell.

Under the present experimental single-collision conditions (see Fig. 2) and, with an ion beam composed of O^- anions, equations for the relevant fractions reduce to:

$$dF_0 = F_{-1}\sigma_{-10}d\vartheta \quad (2)$$

$$dF_{-1} = -F_{-1}(\sigma_{-10} + \sigma_{-11})d\vartheta \quad (3)$$

$$dF_1 = F_{-1}\sigma_{-11}d\vartheta \quad (4)$$

Double electron loss cross-section (σ_{-11}) was estimated by monitoring the yield of O^+ by reversing the AEF polarity confirming to be negligible, as it is the case for other negative species at this energy [44].

Using the signal from the neutral atoms (central CEM), we applied the SGR method, Eq. (2). From the ion beam signal (lateral CEM), we applied the BAT method, Eq. (3). The experiment is carried out as a function of the O_2 gas target thickness $\vartheta = \ell P/\kappa T$. Where ℓ is its effective length, P the pressure, T the temperature of the gas cell and, κ is Boltzmann's constant. Although both measurement methods are expected to yield

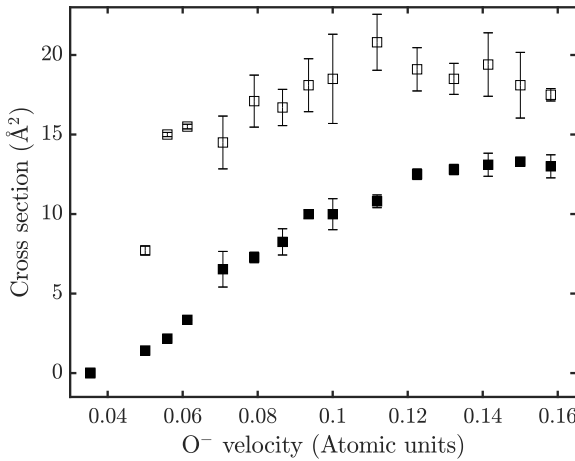


FIG. 3. Present results for the measurements of the collision-induced total electron loss cross sections (CS) for the interaction system: $O^- + O_2$. Measured with BAT method (open squares) were derived from experimental parameters in Eq. (3). Measured with SGR method (closed squares) were derived from Eq. (2).

the same value for σ_{-10} , we use different notations: ${}^s\sigma$ for SGR and, ${}^b\sigma$ for BAT, respectively.

III. RESULTS

The present measurements are shown in Fig. 3. The data dispersion in Fig. 3 is mainly originated by the pressure measurements and the ion beam instability caused by the ion source's plasma fluctuations. In the case of ${}^b\sigma$, the vertical axis is proportional to the ion-beam intensity readings normalized to I_i . In the case of ${}^s\sigma$, the vertical axis is proportional to the initial and final I_i ion-beam currents average. This could be the reason for the difference in the data dispersion.

Below a kinetic energy $E_0 < 4$ keV, CS is lower; consequently, the counting rate signal intensity deteriorated. This effect was averted by increasing the gas cell pressure. This strategy was unfeasible at the higher energy interval because CS was higher and, the signal saturated the counters. This resulted in two different regimes for the statistical error bars in the measurements.

We now turn to the question of the disagreement between ${}^s\sigma$ and ${}^b\sigma$. In BAT, all processes that can extinguish the parent ion beam intensity are accounted for, while in SGR, only neutral atoms resulting from the interaction with O_2 are detected. Although, at first order of the solutions of Eq. (3) and Eq. (2) the values for ${}^s\sigma$ and ${}^b\sigma$ are expected to be the same, the physics involved in each of the measurement methods is different. For instance, double electron loss will not be accounted for in SGR, while it will contribute to BAT. Another process that contributes to CSs is electron transfer, however, this

process is expected to contribute equally to both signals, therefore, it does not explain the discrepancy.

It is important to point out that the disagreement between the electron loss cross sections at the present energy range has been a long-standing question in the field and is not restricted to the present collision system [45]. For instance, a partial review of previous measurements for the same collision system is offered in Fig. 4. Data points measured with BAT (open symbols) are those by Bailey & Mahadevan [46], Hasted & Smith [47] and, Bennet *et al.* [48]. In the cases of Ranjan & Goodyear [49], Comer & Schulz [50] and Mauer & Schulz [51] they measured with techniques based on electron current collection with different calibrations and electron collection schemes.

In these electron current collection techniques an electric or magnetic field is adjusted for maximum current collection and a calibration for the electron-collecting electrodes is performed. No tendency can be established from these data sets, apart from the observation that since they intended to measure the total electron current; their data can be compared, in principle, with BAT.

It is noted in Fig. 3 that the cross-section difference tends to decrease as a function of the particles' speed. We propose that the observed difference in CS can be attributed to the presence of an undetermined auto-detaching state formed during the collision.

Let's define the time of flight t_{of} as the time the ion beam spends through the length of AEF; this time is different for each accelerating energy. At higher energies, t_{of} becomes shorter, and the auto detaching states states have less time to decay. This is the reason why at the higher energy interval of the present study, ${}^b\sigma - {}^s\sigma$ appears to subside. As a consequence, electrons may be lost during the anion's t_{of} to the lateral CEM while in the AEF region, resulting in O atoms not being detected by the central CEM. This explains why they are accounted for by BAT and not by SGR.

To try to test this hypothesis, we offer the following analysis. Let the flux of particles per unit area that the ion beam encounters at speed v in the gas cell be $v\vartheta$. Let the AD states flux be proportional to the difference of the total flux responsible for the attenuation and the flux related to direct detachment. This difference decreases as a function of time:

$$\int_0^\infty v \vartheta^m dt = - \int_0^\infty (\vartheta^b - \vartheta^s) v dt \quad (5)$$

The superscripts m , b and s refer to metastable, BAT, or SGR techniques respectively. At $t \rightarrow \infty$, ${}^mF \approx {}^bF \approx {}^sF$ and Eq. (5) reduced to,

$${}^m\sigma = \frac{{}^s\sigma {}^b\sigma}{{}^b\sigma - {}^s\sigma} \quad (6)$$

Plotting ${}^m\sigma$ versus t_{of} , one obtains Figs. 5 and 6 that show behaviors consistent with the hypothesis of

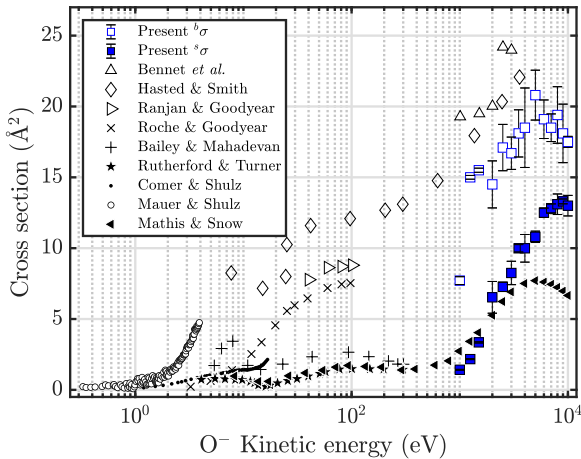


FIG. 4. Partial compilation of electron loss cross sections for the interaction system: $O^- + O_2$ from relevant authors. Present results: BAT ($^b\sigma$), SGR ($^s\sigma$). Bailey & Mahadevan [46], Hasted & Smith [47], Bennet *et al.* [48]. Ranjan & Goodyear [49], Comer & Shulz [50], Mauer & Shulz [51]. Electron transfer cross sections: Mathis & Snow [52] Roche & Goodyear [53], Rutherford & Turner [54].

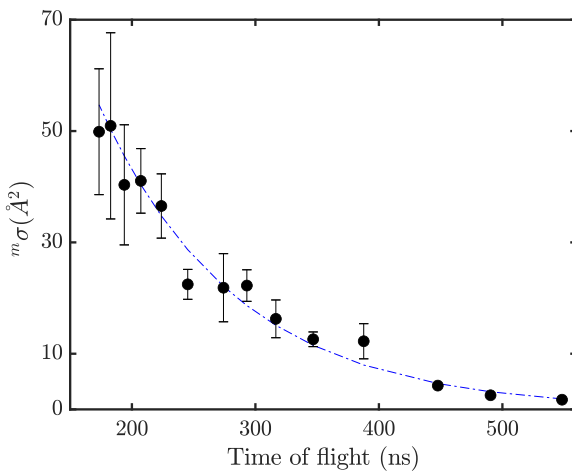


FIG. 5. Auto-detaching CS, $m\sigma$, of the metastable population as a function of the time of flight derived according to Eq. (6) for the interaction system $O^- + O_2 \rightarrow O^* + e^- + O_2^*$. The dashed line represents a minimum square fit to an exponential decay from which a value of 107 ± 15 ns for τ was derived. The error bars represent total uncertainty: the error from the AEF edge effects and the average standard deviation from the numerical fit.

a metastable auto-detaching state population's decay for both gas targets. The cross sections used to derive Fig. 6 were taken from [33]. Both experimental derivations for $m\sigma$ are consistent. We note that the value is lower when the target is N_2 , possibly due to the cross-sections when the target was N_2 being lower and, having an impact on

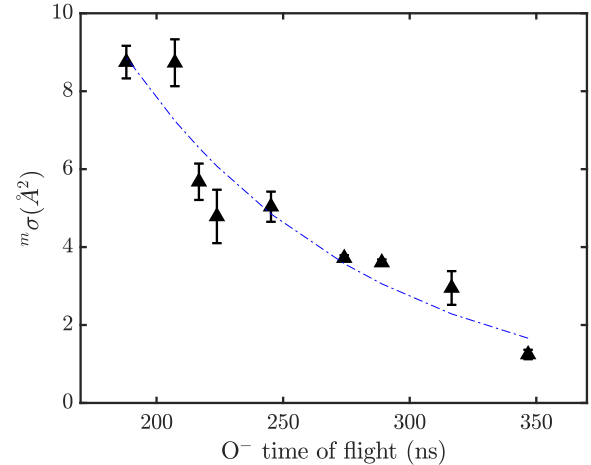


FIG. 6. Auto-detaching CS, $m\sigma$, of the metastable population as a function of the time of flight derived according to Eq. (6) for the interaction system $O^- + N_2 \rightarrow O^* + e^- + N_2^*$. The dashed line represents a minimum square fit to an exponential decay from which a value of 95 ± 13 ns for τ was derived. The error bars represent total uncertainty: the error from the AEF edge effects and the average standard deviation from the numerical fit. The data for the cross sections ($^b\sigma$ and $^s\sigma$) were taken from [33].

the statistical quality of the value. The average for τ is 100 ± 10 ns.

The auto-detachment lifetime can also be assessed by quantum-mechanical methods as explained above. The detachment width is obtained by analytic continuation of the pseudo-spectrum, but the position of the resonance should be determined to obtain the auto-detachment width and consequently the lifetime. So, a separated calculation was done to determine more precisely the 4S ($1s^2 2s^2 2p^3 3s^2$) resonance. This is done with the same approach to obtain the pseudo-spectrum, *i.e.*, at the CASSCF level. The calculated energy was 10.83 eV. This value is certainly overestimated since it has been obtained from the pseudo-spectrum, which is not appropriate for this kind of state, *i.e.* a state immersed in the continuum, due to the use of square-integrable basis set. Experimentally [55], this state was determined as 8.78 eV relative to the oxygen ground state. If we sum to that the value of the measured electron affinity of oxygen, 1.46 eV, we end up with 10.24 eV. This should be compared with the present value of 10.83 eV.

The auto-detachment width (and lifetime) are determined to this transition energy.

IV. CONCLUSIONS

The hypothesis of an auto-detaching state of O^- in the ns time scale is proved against both experiment and theory. The experiment is based on electron loss cross sec-

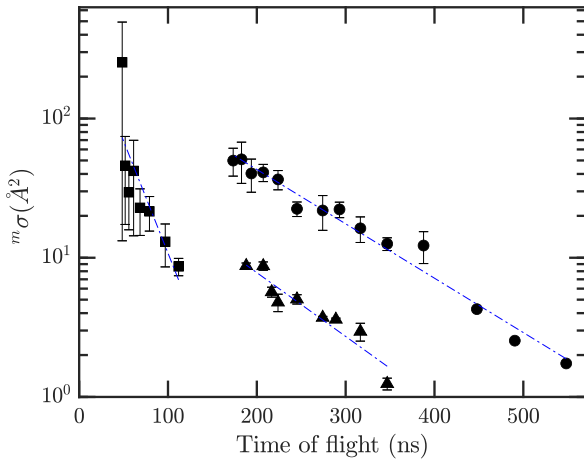


FIG. 7. For comparison, a compilation plot of the auto-detaching CS, $m\sigma$, of the metastable population as a function of the time of flight derived according to Eq. (6) for the present interaction system: \bullet , $O^- + O_2$ (from Fig. 5). $m\sigma$ was also derived for $O^- + N_2$: \blacktriangle , (from Fig. 6, data taken from [33]) and, for $H^- + O_2$, \blacksquare [12]. The dashed lines represent minimum square fits to exponential decays. For the case of $H^- + O_2$, $\tau = 25 \text{ ns} \pm 4 \text{ ns}$.

tions and the time-of-flight spectrometry principle. The

theoretical derivation was developed from the Green's function analytic continuation within the Fano-Feshbach model. Both methods are consistent with the existence of an undetermined population of a metastable auto-detaching state decay with a lifetime τ of $107 \pm 15 \text{ ns}$ (see Fig. 5) and $95 \pm 13 \text{ ns}$ (see Fig. 6) in the experiment and, of 75 ns in the theory, respectively.

The present hypothesis may also help solving the discrepancies among several measurements of the electron loss cross sections at the present energy range.

ACKNOWLEDGMENTS

National Autonomous University of Mexico (UNAM), through the Support Program for the Improvement of the Academic Staff of UNAM (PASPA). The University of Saskatchewan for the facilities provided during GH sabbatical stay. CONAHCyT CF-2023-I-918. Technical support from Guillermo Bustos, Héctor H. Hinojosa, Reyes García, Armando Bustos, Juana A. Romero, and Arturo Quintero. This study was supported in part by the Brazilian agency Fundação de Amparo à Pesquisa do Estado do Rio de Janeiro (FAPERJ), code E-262109342019. The authors also acknowledge Conselho Nacional de Desenvolvimento Científico e Tecnológico (CNPq), Coordenação de Aperfeiçoamento Pessoal de Nível Superior (CAPES).

[1] M. K. Kristiansson, K. Chartkunchand, G. Eklund, O. M. Hole, E. K. Anderson, N. de Ruette, M. Kaminska, N. Punnakayathil, J. E. Navarro-Navarrete, S. Sigurdsson, J. Grumer, A. Simonsen, M. Björkhage, S. Rosén, P. Reinhard, M. Blom, A. Källberg, J. D. Alexander, H. Cederquist, H. Zettergren, H. T. Schmidt, and D. Hanstorp, *Nat. Commun.* **13**, 10.1038/s41467-022-33438-y (2022).

[2] T. Andersen, *Phys. Rep.* **394**, 157 (2004).

[3] D. J. Pegg, *Rep. Prog. Phys.* **67**, 857 (2004).

[4] S. Chandrasekhar, *Astrophys. J.* **100**, 176 (1944).

[5] S. Chandrasekhar, *Rev. Mod. Phys.* **16**, 301 (1944).

[6] D. R. Bates and H. S. W. Massey, *Philos. Trans. R. Soc. London, Ser. A* **239**, 269 (1943).

[7] H. Massey and D. Bates, *Rep. Prog. Phys.* **9**, 62 (1942).

[8] A. R. P. Rau, *Science* **258**, 1444 (1992).

[9] A. R. P. Rau, *J. Astrophys. Astron.* **17**, 113–145 (1996).

[10] H. Berry, *Phys. Scr.* **12**, 5 (1975).

[11] P. Balling, H. Andersen, C. Brodie, U. Pedersen, V. Petrunin, M. K. Raarup, P. Steiner, and T. Andersen, *Phys. Rev. A* **61**, 022702 (2000).

[12] S. Vergara, A. A. Martínez, F. R. Peñalver, and G. Hinojosa, *J. Phys. B: At. Mol. Opt. Phys.* **54**, 155201 (2021).

[13] R. T. Desai, Z. Zhang, X. Wu, and C. Lue, *Planet. Sci. J.* **2**, 99 (2021).

[14] D. Nandi, V. S. Prabhudesai, E. Krishnakumar, and A. Chatterjee, *Rev. Sci. Instrum.* **76**, 053107 (2005).

[15] S. A. Pshenichnyuk, N. Asfandiarov, A. S. Vorob'ev, and Š. Matejčík, *Physics-Uspekhi* **65**, 163 (2022).

[16] J. Xie, X.-F. Gao, M. Fan, H. Li, B. Wu, and S. X. Tian, *Rev. Sci. Instrum.* **95** (2024).

[17] D. Pegg and D. Hanstorp, Photodetachment, in *Springer Handbook of Atomic, Molecular, and Optical Physics* (Springer, 2023) pp. 943–953.

[18] C. C. Jarrold, *ACS Phys. Chem. Au* **3**, 17 (2023).

[19] A. Ayasli, P. Tóth, T. Michaelsen, T. Gstir, F. Zappa, D. Papp, G. Czakó, and R. Wester, *J. Phys. Chem. A* **128**, 3078 (2024).

[20] D. Kim, F. Rizzi, K. W. Cheng, J. Han, F. Bisetti, and O. M. Knio, *Combust. Flame* **162**, 2904 (2015).

[21] N. Popov and S. Starikovskaia, *Prog. Energy Combust. Sci.* **91**, 100928 (2022).

[22] D. Depla, *Crit. Rev. Solid State Mater. Sci.* **49**, 718 (2024).

[23] G. J. Molina-Cuberos, H. Lichtenegger, K. Schwengenbühel, J. J. López-Moreno, and R. Rodrigo, *J. Geophys. Res. Planets* **107**, 3 (2002).

[24] V. Mukundan and A. Bhardwaj, *Astrophys. J.* **856**, 168 (2018).

[25] C. A. Nixon, *ACS Earth Space Chem.* **8**, 406 (2024).

[26] D. Hansen, W. C. Stolte, O. Hemmers, R. Guillemin, and D. W. Lindle, *J. Phys. B: At. Mol. Opt. Phys.* **35**, L381 (2002).

[27] W. C. Stolte, M. Sant'Anna, G. Öhrwall, I. Dominguez-Lopez, M. Piancastelli, and D. W. Lindle, *Phys. Rev. A* **68**, 022701 (2003).

[28] S. Schippers, T. Buhr, A. Borovik Jr, K. Holste, A. Perry-Sassmannshausen, K. Mertens, S. Rein-

wardt, M. Martins, S. Klumpp, K. Schubert, *et al.*, X-Ray Spectrom. **49**, 11 (2020).

[29] T. Brage and J. Grumer, J. Phys. B: At. Mol. Opt. Phys. **50**, 025001 (2016).

[30] V. A. Esaulov, Autodetaching states of atomic negative ions (2017), arXiv:1707.07661 [physics.atom-ph].

[31] A. K. Edwards, J. S. Risley, and R. Geballe, Phys. Rev. A **3**, 583 (1971).

[32] A. Schlachter, M. Sant'Anna, A. Covington, A. Aguilar, M. Gharaibeh, E. Emmons, S. Scully, R. Phaneuf, G. Hinojosa, I. Álvarez, *et al.*, J. Phys. B: At. Mol. Opt. Phys. **37**, L103 (2004).

[33] A. Martínez-Calderón, M. Sant'Anna, and G. Hinojosa, Phys. Rev. A **109**, 032806 (2024).

[34] G. W. F. Drake, Astrophys. J. **184**, 145 (1973).

[35] C. F. Bunge, M. Galán, R. Jáuregui, and A. V. Bunge, Nucl. Instrum. Methods Phys. Res. **202**, 299 (1982).

[36] M. Bylicki and E. Bednarz, Phys. Rev. A **67**, 022503 (2003).

[37] R. R. Corderman and W. C. Lineberger, Annu. Rev. Phys. Chem. **30**, 347 (1979).

[38] A. Oliveira, G. Jalbert, and A. Rocha, J. Chem. Phys. **156**, 244116 (2022).

[39] B. N. C. Tenorio, M. A. C. Nascimento, and A. B. Rocha, J. Chem. Phys. **149**, 074104 (2018).

[40] L. G. Christoforou, The lifetimes of metastable negative ions, in *Advances in Electronics and Electron Physics* (Academic Press, 1978) pp. 56–125.

[41] Beam Imaging Solutions Inc., (2025), <http://www.beamimaging.com/> (accessed August 13, 2025).

[42] E. M. Hernández, L. Hernández, C. Martínez-Flores, N. Trujillo, M. Salazar, A. Chavez, and G. Hinojosa, Plasma Sources Sci. Technol. **23**, 015018 (2014).

[43] M. E. W, M. J. B. A, and R. M. E, *Atomic Collisions, Heavy Particle Projectiles* (Wiley, New York, 1993).

[44] E. Hernández, L. Hernández, L. Serkovic-Loli, and G. Hinojosa, Int. J. Mass Spectrom. **403**, 39 (2016).

[45] F. Rahman and B. Hird, At. Data Nucl. Data Tables **35**, 123 (1986).

[46] T. L. Bailey and P. Mahadevan, J. Chem. Phys. **52**, 179 (1970).

[47] J. B. Hasted and R. A. Smith, Proc. R. Soc. Lond. A **235**, 349 (1956).

[48] R. A. Bennett, J. T. Moseley, and J. R. Peterson, J. Chem. Phys. **62**, 2223 (1975).

[49] R. Ranjan and C. C. Goodyear, J. Phys. B: At. Mol. Phys. **6**, 1070 (1973).

[50] J. Comer and G. J. Schulz, Phys. Rev. A **10**, 2100 (1974).

[51] J. L. Mauer and G. J. Schulz, Phys. Rev. A **7**, 593 (1973).

[52] R. F. Mathis and W. R. Snow, J. Chem. Phys. **61**, 4274 (1974).

[53] A. E. Roche and C. C. Goodyear, J. Phys. B: At. Mol. Phys. **2**, 191 (1969).

[54] J. A. Rutherford and B. R. Turner, J. Geophys. Res. (1896-1977) **72**, 3795.

[55] D. Spence, Phys. Rev. A **12**, 721 (1975).